Precision Measurement Method for Cryogenic Amplifier Noise Temperatures Below 5 K

James Randa, *Senior Member, IEEE*, Eyal Gerecht, *Member, IEEE*, Dazhen Gu, *Student Member, IEEE*, and Robert L. Billinger

***Abstract*—We report precision measurements of the effective input noise temperature of a cryogenic (liquid-helium temperature) monolithic-microwave integrated-circuit amplifier at the amplifier reference planes within the cryostat. A method is given for characterizing and removing the effect of the transmission lines between the amplifier reference planes and the input and output connectors of the cryostat. In conjunction with careful noise measurements, this method enables us to measure amplifier noise temperatures below 5 K with an uncertainty of 0.3 K. The particular amplifier that was measured exhibits a noise temperature below 5.5 K from 1 to 11 GHz, attaining a minimum value of 2.3 K±0.3 K at 7 GHz. This corresponds to a noise figure of 0.034 dB±0.004 dB. The measured amplifier gain is between 33.4 dB±0.3 dB and 35.8 dB±0.3 dB over the 1–12-GHz range.**

***Index Terms*—Amplifier noise, cryogenic monolithic-microwave integrated-circuit (MMIC) amplifier, noise measurement, noise temperature, thermal noise.**

I. Introduction

A. Background and Motivation

CRYOGENIC low-noise amplifiers (LNAs) have been important in radio astronomy for some time [1], [2], [3]. They have been used as the first stage of receivers at microwave frequencies and in IF sections following mixers at millimeter-wave and sub-millimeter-wave frequencies. Recently, they have assumed added importance as IF amplifiers in terahertz applications. The development over the past decade of near-quantum-limited heterodyne detectors for terahertz frequencies, such as hot electron bolometer (HEB) receivers [4], has made possible very low noise receivers for a range of terahertz applications, including imaging utilizing multipixel focal plane arrays (FPAs) for biomedical and homeland security uses, and spectroscopy instrumentation for biomedical applications and astrophysical observations. In all these applications, whether in past or present radio astronomy or in terahertz receivers for terrestrial applications, the noise performance of the LNA is crucial. The need for ultra-low-noise (less than 15 K) amplifiers in these applications has driven the development of a new family of cryogenic amplifiers. The use of InP high electron-mobility transistors (HEMTs) and recent advances in modeling and fabrication technologies have resulted in monolithic-microwave integrated-circuit (MMIC) LNAs with remarkable noise performance (less than 10 K) and low dc-power consumption [5]–[7]. Characterization of the noise properties of these and other cryogenic LNAs presents a significant measurement challenge in terms of accounting for the small noise contributions from components mismatches and losses. Current methods have typical uncertainties of approximately 1 K or more [7]. This paper demonstrates a method for accurate measurements of the very low noise temperatures (below 5 K) that can be achieved by present cryogenic LNAs. The method is not quick, efficient, or easy; but it does offer very small uncertainties. At frequencies for which the "matched" loads have small reflection coefficients, the standard uncertainty ($1\ \sigma$) in the amplifier's noise temperature is ±0.3 K. The method uses measurements on the external room-temperature ports of the cryostat to determine the gain between the two cryostat ports. A series of separate measurements is used to characterize the lines between the amplifier and cryostat's external ports. The amplifier's noise temperature is then determined by measurements with an internal liquid-helium-temperature matched load on the input of the amplifier.

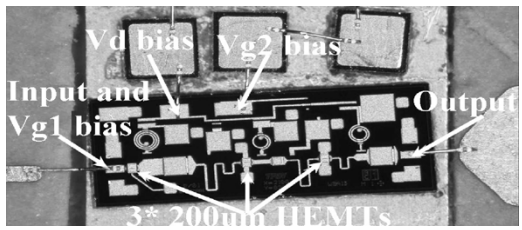

Fig. 1. Cryogenic InP HEMT LNA.

B. Amplifier

The MMIC LNA chip under test was developed by Weinreb and Wadefalk at the Jet Propulsion Laboratory (JPL), California Institute of Technology, Pasadena. This amplifier has three stages of InP transistors with 0.1-μm gate length, demonstrated gain of approximately 10 dB per stage, and total noise temperature expected to be less than 10 K throughout the 1–10-GHz band and relatively independent of bias settings [7], [8]. Fig. 1 shows the MMIC chip (size 0.75 × 2 mm). The three capacitors shown on top are the pads for dc bias of the transistors. Both the input and output pads are wire (ribbon) bonded to microstrip transmission lines placed at either end of the circuit.

Manuscript received August 16, 2005; revised November 12, 2005. This work was supported in part by the U.S. Department of Commerce under the National Institute of Standards and Technology Advanced Technology Program.

The authors are with the Electromagnetics Division, National Institute of Standards and Technology, Boulder, CO 80305 USA (e-mail: randa@boulder.nist.gov; gerecht@boulder.nist.gov; dau@boulder.nist.gov; bilinger@boulder.nist.gov).

Digital Object Identifier 10.1109/TMTT.2005.864107

Fig. 2. Cryogenic measurement setup for the MMIC LNA. The LNA is in the center under the metal strap.

The MMIC LNA chip is mounted in an amplifier block with input and output subminiature A (SMA) connectors. The amplifier block is mounted on the cold plate with indium sheets to optimize the thermal contact. The cold plate and, therefore, the amplifier block are cooled to an ambient temperature of 4.1 K in a cryogenic Dewar (see Fig. 2).

II. Theory

A. Noise Temperature

At the outset, we should clarify the definition of the amplifier noise temperature that we will use. In many amplifier noise measurements at microwave frequencies, one can ignore some technicalities with impunity, but for the very small temperatures and even smaller uncertainties that we will deal with, it is necessary to exercise extra care. The basic defining equation is that the output noise temperature is given by

$$T_{\text{out}} = G\left(T_{\text{in}} + T_e + \frac{hf}{2k_B}\right) \tag{1}$$

where G is the available gain of the amplifier, T_{in} is the noise temperature of the input termination, T_e is the effective input noise temperature of the amplifier, h is Planck's constant, f is the frequency, and k_B is the Boltzmann's constant. The available gain G and the effective input noise temperature T_e both depend on the reflection coefficient (or impedance) of the input termination and are also a function of frequency. In the present measurements, we consider only the case of matched (reflectionless) input terminations for the amplifier so that the measured amplifier noise temperature corresponds to the noise figure for reflectionless input terminations. The temperatures appearing in (1) and elsewhere throughout this paper are *noise* temperatures rather than physical temperatures unless otherwise stated. They are defined as the available noise spectral power divided by Boltzmann's constant so that, for a passive termination, the noise temperature T is given by the familiar Planck form

$$T = \frac{1}{k_B}\left(\frac{hf}{e^{hf/(k_B T_{\text{phys}})} - 1}\right) \tag{2}$$

where T_{phys} is the physical temperature.

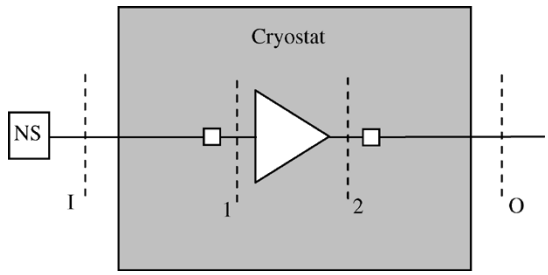

Fig. 3. Configuration and reference planes for amplifier and cryostat. NS denotes noise source.

The aspect of (1) that may be unfamiliar to some is the appearance of the $hf/2k_B$ term. This is the contribution to the input noise due to quantum vacuum fluctuations [9]–[11]. For convenience, we define $T_{\text{vac}} \equiv hf/(2k_B)$. Normally it is not a concern at microwave frequencies, and certainly not in the 1–12-GHz range, where T_{vac} ranges from 0.024 to 0.29 K. However, since we are dealing with such low temperatures, and because our uncertainties will be about 0.3 K, it is necessary to account for this term. There is some question whether T_{vac} should be included in the input noise temperature or whether it should be attributed to the amplifier and included in T_e. We adopt the convention that it is present at the input of the amplifier [12] so that it is *not* included in T_e. We depart from [12] in that we do not include T_{vac} in the noise temperature of a passive termination (2) and, therefore, it appears explicitly in (1). This difference has no effect on the results.

B. Calculations

We consider the case of matched (i.e., reflectionless) input terminations, and we refer to the amplifier's effective input noise temperature for this case as T_e. Before immersing ourselves in algebraic details, we preview the general measurement plan. Figs. 3 and 4 show the measurement configurations to be used. We shall refer to a configuration by the number of the figure representing it. A standard hot/cold measurement (detailed below) on configuration 3 is used to determine the gain at the cryostat ports (outside the cryostat at room temperature). A similar hot/cold measurement on configuration 4(a) determines the losses in the lines, permitting us to extract the amplifier gain from the gain at the cryostat ports. Configurations 4(b) and (c) are used to measure how much noise is added by each section of transmission line within the cryostat. Finally, in configurations 4(d) and (e), a matched load at liquid-helium temperature is connected directly to the amplifier's input, which allows us to measure T_e, given the earlier measurements of amplifier gain and the characteristics of the transmission lines.

The relevant reference planes are shown in Fig. 3. Planes I and O are the input and output planes of the cryostat, at room temperature, and planes 1 and 2 are at the input and output of the amplifier, within the cryostat and, therefore, at liquid-helium temperature. The cryostat planes I and O are accessible for measurements, whereas we wish to determine the amplifier gain and noise temperature at the amplifier planes 1 and 2. We must therefore characterize the transmission lines between I and 1 and between 2 and O, and we must correct for their effects.

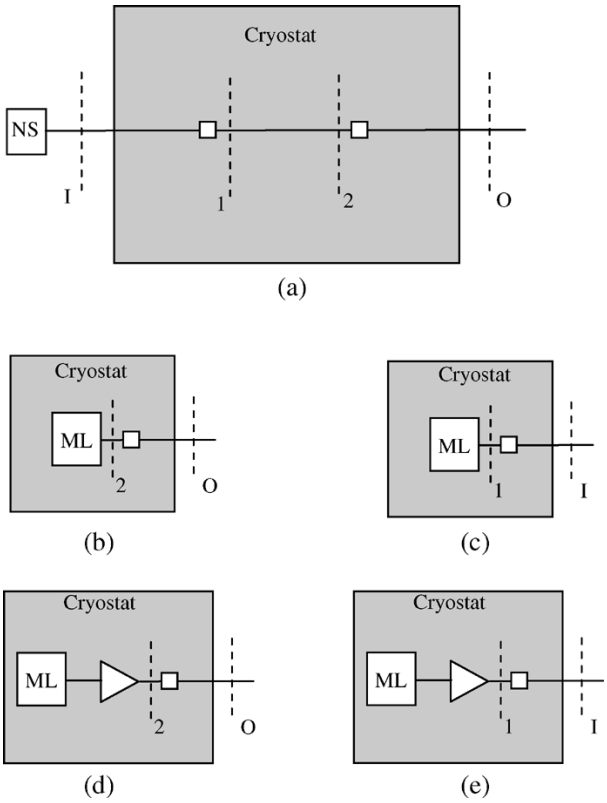

Fig. 4. Additional measurement configurations. ML denotes matched load and NS denotes noise source.

The small blocks near planes 1 and 2 represent the location of the internal connectors relative to those planes.

Since we will measure output noise temperatures at plane O, and we will use known input noise temperatures at plane I, the characterization that is required is the relationship between noise temperatures at I and 1, and at O and 2. The noise temperature at O (T_O) is related to that at 2 (T_2) by

$$T_O = \alpha_{O2} T_2 + \Delta T_2 \tag{3}$$

where α_{O2} is the available-power ratio from plane 2 to plane O, and ΔT_2 is the cumulative noise added by the line in going from liquid-helium temperature at plane 2 to room temperature at plane O. An important point is that ΔT_2 depends on the direction: it is different going from 2 to O from what it is going from O to 2. This may seem counter-intuitive at first, but it becomes less so if one considers the case of two attenuators at different temperatures and computes the output noise temperature in the two directions for the same input noise temperature. (It is similar to computing the noise temperature of cascaded amplifiers for different ordering of the amplifiers.) To deal with the direction dependence, we adopt the convention that the unprimed ΔT_1 and ΔT_2 will be used for the direction from inside the cryostat to the outside (plane 1 to plane I, and 2 to O), and $\Delta T_1'$ and $\Delta T_2'$ will be used for the opposite direction, from outside in.

In general, α also depends on the direction, and in particular it depends on the reflection coefficient of the termination of the input end. In principle, we are working with matched terminations so that the input reflection coefficients should be very near zero, and α_{I1} and α_{O2} will not change from one configuration to another. In practice, the matched loads are far from perfect, particularly at 4.1 K and S_{22} of the amplifier can be sizable. We must therefore exercise some care for the α's occurring in Figs. 3 and 4. The required care is exercised in the Appendix, where we show

$$\begin{aligned}
\alpha_{O2}(3) &\approx \alpha_2 \frac{\left(1 - \dfrac{|\Gamma_O(3)|^2}{\alpha_1\alpha_2}\right)}{\left(1 - |\Gamma_O(3)|^2\right)} \\
\alpha_{O2}(4d) &\approx \alpha_2 \frac{\left(1 - \dfrac{|\Gamma_O(4d)|^2}{\alpha_1\alpha_2}\right)}{\left(1 - |\Gamma_O(4d)|^2\right)} \\
\alpha_{I1}(4e) &\approx \alpha_1 \frac{\left(1 - \dfrac{|\Gamma_I(4e)|^2}{\alpha_1\alpha_2}\right)}{\left(1 - |\Gamma_I(4e)|^2\right)}
\end{aligned} \tag{4}$$

where α_1 and α_2 are the values for configuration 4(a).

In Fig. 3, if a reflectionless noise source of noise temperature T_{in} is connected to plane I, then the noise at the output plane O will be given by

$$\begin{aligned}
T_O(3) &= \alpha_{O2}(3) G (T_1 + T_e + T_{\text{vac}}) + \Delta T_2 \\
&= \alpha_1 \alpha_{O2}(3) G T_{\text{in}} + \alpha_{O2} G \Delta T_1' \\
&\quad + \alpha_{O2}(3) G (T_e + T_{\text{vac}}) + \Delta T_2
\end{aligned} \tag{5}$$

where G is the available gain of the amplifier (between planes 1 and 2) for $\Gamma_{\text{in}} = 0$. (We neglect the small reflections introduced by the connections at plane I and to the left of plane 1 so that a reflectionless input termination at I results in a reflectionless termination at the amplifier's input plane 1.) The quantities of interest in (5) are T_e and G, which must be disentangled from the line parameters α_1, α_{O2}, $\Delta T_1'$, and ΔT_2. Measurements with two different input noise sources T_h and T_c, as in the standard Y-factor method, allow determination of the gain at the cryostat ports $\alpha_1\alpha_{O2}(3)G$. We then use (4) to relate $\alpha_{O2}(3)$ to α_2 and obtain

$$\alpha_1\alpha_2 G = \frac{T_O(3,h) - T_O(3,c)}{T_h - T_c} \frac{\left(1 - |\Gamma_O(3)|^2\right)}{\left(1 - \dfrac{|\Gamma_O(3)|^2}{\alpha_1\alpha_2}\right)} \tag{6}$$

where $(3,h)$ and $(3,c)$ refer to configuration 3 with hot and cold input noise sources. We could also determine the intercept $[\alpha_2(3) G \Delta T_1' + \alpha_2 G T_e + \Delta T_2]$, but we do not use that information. To obtain G from (6), we must then determine $\alpha_1\alpha_2$.

The configurations for the additional measurements are shown in Fig. 4. Fig. 4(a) is similar to Fig. 3, but with the amplifier replaced by a short through section. For a noise temperature T_{in} connected at port I, the noise temperature at port O is given by

$$T_O(4a) = \alpha_1\alpha_2 T_{\text{in}} + \alpha_2 \Delta T_1' + \Delta T_2 \tag{7}$$

where we neglect any loss in the short section of through (at liquid-helium temperature) between planes 1 and 2 (a very good

assumption based on measurements of the through section at room temperature). Measurement of this configuration with two different values of $T_{\rm in}$ allows us to determine $\alpha_1\alpha_2$

$$\alpha_1\alpha_2 = \frac{T_O(4a,h) - T_O(4a,c)}{T_h - T_c}. \tag{8}$$

It also determines $\alpha_2\Delta T_1' + \Delta T_2$, but again, we will not use this. As a check, this configuration is measured in both directions, measuring the noise temperatures at O for two different noise sources connected at I, and measuring the noise temperatures at I for two different noise sources connected at O. We then can use (8) in conjunction with (6) to determine the amplifier gain G.

In Fig. 4(b) and (c), a matched load is connected directly to one of the internal connectors, either plane 1 or plane 2. In these cases, the output noise temperatures are given by

$$\begin{aligned} T_I(4c) &= \alpha_{I1}(4c)T_{He} + \Delta T_1 \\ T_O(4b) &= \alpha_{O2}(4b)T_{He} + \Delta T_2 \end{aligned} \tag{9}$$

where T_{He} is the liquid-helium temperature, as measured by the GRT. Since T_{He} is small, (9) provides a good direct determination of ΔT_1 and ΔT_2 even if the uncertainties in α_1 and α_2 are rather large, provided that we can measure T_I and T_O well. In fact, we shall see in the uncertainty analysis below that it is sufficient to use $\alpha_1 \approx \alpha_2 \approx \sqrt{\alpha_1\alpha_2}$ in (9). For ΔT_1 and ΔT_2, we then have

$$\begin{aligned} \Delta T_1 &= T_I(4c) - \sqrt{\alpha_1\alpha_2}T_{He} \\ \Delta T_2 &= T_O(4b) - \sqrt{\alpha_1\alpha_2}T_{He} \end{aligned} \tag{10}$$

where $\alpha_1\alpha_2$ is given by (8).

In Fig. 4(d) and (e), a matched load is connected to the input of the amplifier, inside the cryostat. The output noise temperatures in these cases are given by

$$\begin{aligned} T_I(4e) &= \alpha_{I1}(4e)G(T_{He} + T_e + T_{\rm vac}) + \Delta T_1 \\ T_O(4d) &= \alpha_{O2}(4d)G(T_{He} + T_e + T_{\rm vac}) + \Delta T_2. \end{aligned} \tag{11}$$

Since we can determine the product $\alpha_1\alpha_2$, but we do not have a good method for measuring α_1 and α_2 individually, we combine the two equations of (11) to yield

$$\begin{aligned} &\alpha_{I1}(4e)\alpha_{O2}(4d)G^2(T_{He} + T_e + T_{\rm vac})^2 \\ &\qquad = [T_I(4e) - \Delta T_1]\,[T_O(4d) - \Delta T_2]\,. \end{aligned} \tag{12}$$

The preceding measurements have already determined $\alpha_1\alpha_2$, G, ΔT_1, and ΔT_2, and thus we can use (12) to determine the amplifier's effective input noise temperature T_e

$$T_e = \left\{ \frac{[T_I(4e) - \Delta T_1]\,[T_O(4d) - \Delta T_2]}{\alpha_{I1}(4e)\alpha_{O2}(4d)G^2} \right\}^{\frac{1}{2}} - T_{He} - T_{\rm vac} \tag{13}$$

where $\alpha_{I1}(4e)\alpha_{O2}(4d)$ is related to $\alpha_1\alpha_2$ by (4).

III. Measurements

A. Setup and Procedures

The input and output ports of the cryostat, as well as the internal ports, had SMA connectors. Adapters were connected to the SMA input and output ports of the cryostat so that all measurements were made with GPC-7 connectors. This was done to minimize concerns about connector repeatability. These adapters remained in place throughout the course of the measurements; they were not removed and reconnected. Since the amplifier itself had SMA connectors, the internal connectors of the cryostat (near planes 1 and 2) were left as SMA. Water jackets were constructed and fitted around the input and output ports of the cryostat to stabilize and maintain these ports at room temperature (23 °C physical temperature). Internal cables of the cryostat were ordinary stainless-steel semirigid cables with Teflon dielectric.

The noise measurements were all performed on the National Institute of Standards and Technology (NIST) coaxial radiometer NFRad [13], and therefore the measurand was the noise temperature. NFRad is an isolated double-sideband total-power radiometer that compares the noise power from the device-under-test to that from two primary standards, one at liquid-nitrogen temperature and one near ambient temperature. Full corrections are made for mismatches and path differences. The mixing is performed at baseband, and the bandwidth of each sideband is 5 MHz. The system noise temperature and gain depend on frequency; typical values are a gain of 100 dB and a noise temperature of 450 K at 8 GHz. The standard uncertainty in the noise-temperature measurement depends on the noise temperature. For noise temperatures in the 1000–15 000-K range, the standard uncertainty is about 0.4% or 0.5% of the noise temperature. For higher temperatures, such as those at the output of the amplifier, a characterized attenuator must be used at the radiometer input, increasing the uncertainty somewhat. For noise temperatures below 100 K, the standard uncertainty is typically between 1.0 and 1.5 K.

The noise measurements required that we first measure relevant reflection coefficients. These measurements were performed using a commercial vector network analyzer (VNA). The procedure was to first cool the cryostat until the temperature of the internal cold plate stabilized at about 4.1 K. The temperature was measured by a germanium resistance thermometer (GRT) mounted on the cold plate. A silicon thermometer was also mounted on the plate and was used for verification purposes. For measurement configurations that included the amplifier, the amplifier was always biased with the same gate and drain voltages ($V_g = 1$ V, $V_d = 1.4$ V), resulting in an operating current of about 17 mA, which corresponds to the maximum gain. The reflection coefficient at the measurement planes (I and/or O) were then measured on the VNA for each of the input sources to be used. For the amplifier measurements of Fig. 3, two input sources were used, a matched load at room temperature and a cryogenic (liquid nitrogen) noise source, whose noise temperature was measured separately. Two different input noise sources were also used in the line measurements of Fig. 4(a), but in this case, they

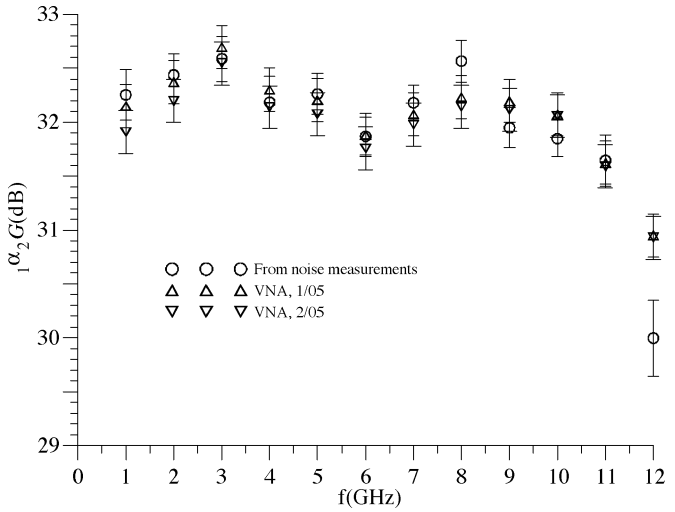

Fig. 5. Measurement results for $\alpha_1\alpha_2 G(\approx G(OI))$ from noise and VNA measurements.

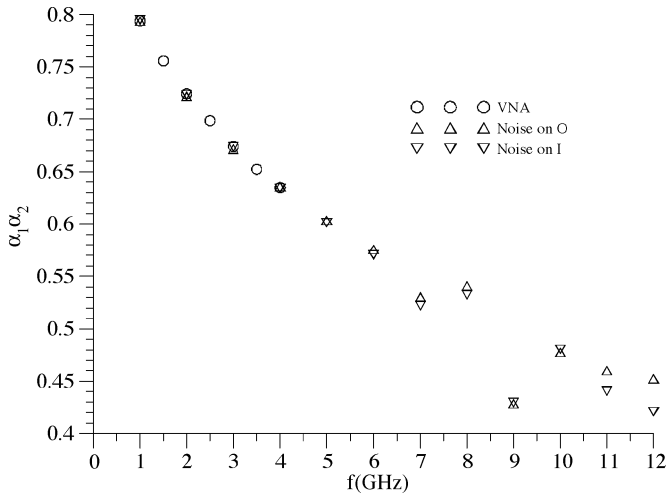

Fig. 6. Measurement results for $\alpha_1\alpha_2$ (dimensionless), from noise and VNA measurements.

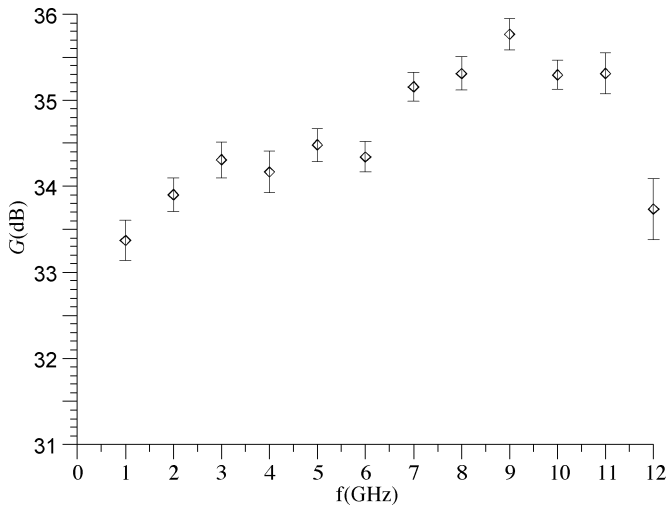

Fig. 7. Measurement results for the amplifier gain between planes 1 and 2.

were the ambient temperature matched load and a commercial diode noise source, whose noise temperatures we had previously measured at the frequencies of interest. After the VNA measurements, the cryostat was moved to NFRad for the noise measurements. Measurements were made from 1 to 12 GHz at 1-GHz intervals. NFRad uses four different receiving modules to cover 1–12 GHz, with the break points occurring at 2, 4, and 8 GHz. At these three overlap frequencies, all measurements were performed with both receiver modules as a check of consistency and repeatability.

In principle, the measurement configurations of Figs. 3 and 4 require four different internal configurations of the cryostat and thus could be accomplished with four separate cooling-warming cycles. The first cycle can be devoted to the hot/cold measurements on configuration 3, and the second cycle can be used for the hot/cold measurements on configuration 4(a). Configurations 4(b) and (e) can be accommodated simultaneously in the cryostat, and therefore they both can be measured in the third cooling-warming cycle. And finally, configurations 4(c) and (d) can also coexist simultaneously in the cryostat, and therefore they both can be measured in the fourth cooling-warming cycle. The ordering of the four cycles is not important, but we chose to measure configuration 3 first, in order to verify that the amplifier was operating as expected. (In practice, of course, more than four cooling–warming cycles were needed due to scheduling, availability of liquid helium, etc.)

B. Results and Checks

Measurements on configuration 3, with two different input noise sources, yield values for $\alpha_1\alpha_2 G$ from (6). As a check of our results, we also measured the S-parameters at cryostat ports I and O, from which we computed the available gain, from I to O, which should be approximately equal to $\alpha_1\alpha_2 G$, $\alpha_1\alpha_2 G \approx G(OI) = |S_{21}|^2/(1-|S_{22}|^2)$ for a matched termination on I. Fig. 5 plots the results for both $\alpha_1\alpha_2 G$ (labeled "noise measurement") and for two separate VNA measurements of $G(OI)$, taken about one month apart (and labeled "VNA"). In this and subsequent graphs, the error bars correspond to the standard uncertainty (1 σ) [14]. For the noise measurement, the uncertainty analysis is given in Section III-C. The VNA uncertainties are estimates based on the manufacturer's values. The manufacturer's values extend only up to gains of 10 dB, where they are about ± 0.1 dB. The values used in Fig. 5 are ± 0.2 dB. The noise and VNA results are generally in good or very good agreement, except at 12 GHz, where they differ by about 0.9 dB.

In a similar manner, measurements on configuration 4(a), using two different input noise sources, can be used in (8) to determine $\alpha_1\alpha_2$. In the Appendix, we show that $\alpha_1\alpha_2$ should be approximately independent of direction (I to O versus O to I), and so we measured it in both directions as a check. As an additional check, the S-parameters between I and O were measured with the VNA from 1 to 4 GHz, and the available gain ($\approx \alpha_1\alpha_2$) was computed, similar to the treatment above of $\alpha_1\alpha_2 G$. All three sets of results are plotted in Fig. 6. Error bars are not shown because they are the approximate size of the symbols. Very good agreement is seen, except at 11 and 12 GHz, where the difference between the measurements in the two directions is 0.02 and 0.03. This discrepancy will be discussed below when we treat the uncertainties. The value of

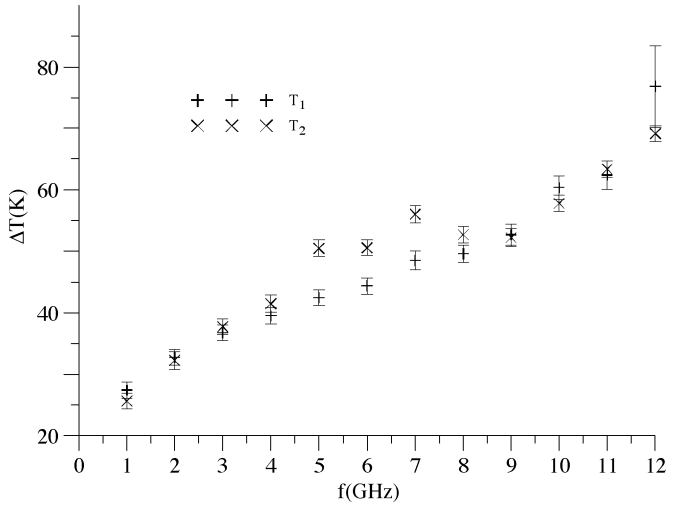

Fig. 8. Measurement results for ΔT_1 and ΔT_2.

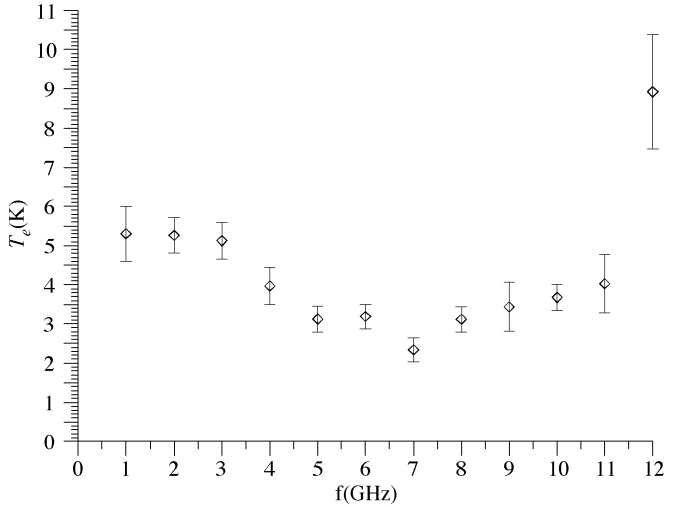

Fig. 9. Effective input noise temperature of amplifier as a function of frequency.

$\alpha_1\alpha_2$ used in the rest of the computations is the average of the measurements in the two directions.

Combining the results for $\alpha_1\alpha_2 G$ with those for $\alpha_1\alpha_2$, we can compute G, which is plotted in Fig. 7. The gain is between 33 and 36 dB throughout the measurement range, and the measurement uncertainties are about 0.15 dB.

The values of ΔT_1 and ΔT_2 were determined from measurements on configurations 4(b) and (c), using (10), and they are plotted in Fig. 8. Two independent measurements of ΔT_1 were performed, with a disconnect/reconnect at plane 1, in order to test the repeatability of the connections and measurements. The average of those two measurements is shown in Fig. 8, and the difference is included as a type-A uncertainty. The relatively large error bar on ΔT_1 at 12 GHz is due to a disparity between the two measurements. Both ΔT_1 and ΔT_2 are seen to increase with frequency from about 25 K at 1 GHz to about 75 K at 12 GHz. The values for ΔT_1 and ΔT_2 are nearly equal, except from 5 to 7 GHz and at 12 GHz. The disparity from 5 to 7 GHz is suspicious. It could be due to a real difference between the two lines or it could be due to a faulty internal connection or some other problem with one measurement. Fortunately, a difference of 10 or 20 K in ΔT_1 or ΔT_2 has virtually no effect on our results for T_e. This can be seen by referring to (11) and (13). ΔT_1 and ΔT_2 enter only as relatively small corrections to $T_I(4d)$ and $T_O(4e)$, both of which are in the range of 15 000–20 000 K and have uncertainties in excess of 100 K. Consequently, we need to know ΔT_1 and ΔT_2 only to within about 50 K.

Finally, the measurements on configurations 4(d) and (e) are used in (13), along with the values already obtained for $\alpha_1\alpha_2 G$, $\alpha_1\alpha_2$, ΔT_1, and ΔT_2, to obtain the amplifier's effective input noise temperature, which is plotted in Fig. 9. The measured noise temperature is below 5.5 K from 1 to 11 GHz, rising to about 9 K at 12 GHz. The lowest value is attained at 7 GHz where $T_e = 2.3\ \text{K} \pm 0.3\ \text{K}$. (For those accustomed to noise figure in decibels, this corresponds to 0.034 dB±0.004 dB.) Uncertainties throughout the range are approximately 0.3 K at frequencies were the matching was good, and higher at frequencies where the matching was poor. The measurement results for G and T_e are tabulated in Table I. The uncertainties in this table are

TABLE I
RESULTS FOR G AND T_e WITH STANDARD UNCERTAINTIES (1σ)

f(GHz)	G(dB)	T_e(K)
1	33.4 ± 0.3	5.3 ± 0.7
2	33.9 ± 0.2	5.3 ± 0.5
3	34.3 ± 0.2	5.1 ± 0.5
4	34.2 ± 0.3	4.0 ± 0.5
5	34.5 ± 0.2	3.1 ± 0.3
6	34.3 ± 0.2	3.2 ± 0.3
7	35.1 ± 0.2	2.3 ± 0.3
8	35.3 ± 0.2	3.1 ± 0.3
9	35.8 ± 0.3	3.4 ± 0.6
10	35.3 ± 0.2	3.7 ± 0.3
11	35.3 ± 0.4	4.0 ± 0.7
12	33.7 ± 0.5	8.9 ± 1.5

the standard uncertainties, corresponding to one standard deviation, computed in accordance with [14]. Care should be taken in comparing uncertainties from other sources, who often quote "3-σ" uncertainties. In such comparisons, one should also be careful that all major components of uncertainty are included.

C. Uncertainties

When measuring such small amplifier noise temperatures, it is obviously essential to evaluate and understand the uncertainties. A detailed uncertainty analysis was performed for both G and T_e; here we present only a summary of the most important components.

We determined G from the ratio of $\alpha_1\alpha_2 G$, using (6), with $\alpha_1\alpha_2$ determined from (8). In addition, there are possible errors due to the fact that we assume, but obviously cannot achieve, perfect matching conditions. This is an important, even dominant, contribution to the uncertainty [15]. The relative uncertainty in G is therefore given by

$$\frac{u(G)}{G} = \sqrt{\frac{u^2(\alpha_1\alpha_2 G)}{(\alpha_1\alpha_2 G)^2} + \frac{u^2(\alpha_1\alpha_2)}{(\alpha_1\alpha_2)^2} + \frac{u_{\text{ML}}^2(G)}{G^2}} \qquad (14)$$

where $u_{\text{ML}}(G)$ is the uncertainty in G due to imperfect matching. We estimated $u_{\text{ML}}(G)$ by taking the difference be-

tween the full expression for available gain and the expression for the matched case using measured magnitudes of reflection coefficients or reasonable approximations, and averaging (rms) over relative phases. This leads to a value for $u_{\rm ML}(G)/G$ of between 0.6% and 6%, depending on frequency.

The uncertainty in $\alpha_1\alpha_2 G$, $u(\alpha_1\alpha_2 G)$, is the other major contribution to (14). If we let $\Delta T_O \equiv T_O(3,h) - T_O(3,c)$ and $\Delta T_{\rm in} \equiv T_a - T_c$, where $T_a = 296.15$ K is the ambient temperature, then from (6) the fractional uncertainty in $\alpha_1\alpha_2 G$ takes the form

$$\frac{u(\alpha_1\alpha_2 G)}{\alpha_1\alpha_2 G} = \sqrt{\frac{u^2(\Delta T_O)}{\Delta T_O^2} + \frac{u^2(\Delta T_{\rm in})}{\Delta T_{\rm in}^2} + \frac{u_{\rm ML}^2(\alpha_1\alpha_2 G)}{(\alpha_1\alpha_2 G)^2}} \tag{15}$$

where $u_{\rm ML}$ again refers to the uncertainty due to imperfect matching conditions. The term due to imperfect matching is estimated in the same manner as in (14), and this fractional uncertainty is found to be between 1% and 7%. The other major contribution to $u(\alpha_1\alpha_2 G)$ in (15) is $u(\Delta T_O)$, and it, is dominated by the uncertainty in $T_O(3,h)$, $u(\Delta T_O) \approx u(T_O(3,h))$. The output noise temperatures $T_O(3,h)$ and $T_O(3,c)$ were measured on the NIST coaxial radiometer NFRad [11], through a 20-dB attenuator, in order to keep the output temperature in the linear range of the radiometer. The fractional type-B uncertainties in these measurements, including the uncertainty introduced by the attenuator, are about 0.6%. However, at the "overlap points" (2, 4, and 8 GHz), where the measurements were repeated, using two different receiving modules, the difference between the two measurements was often significantly larger than 0.6%. To account for this, we added an effective type-A uncertainty equal to the average magnitude of the difference for the given set of measurements. This type-A fractional uncertainty was 2% for $T_O(3,h)$ and $T_O(3,c)$. This resulted in a fractional uncertainty of 3%–4% in ΔT_O and therefore in $\alpha_1\alpha_2 G$ as well. Combining the components in (15) yields a fractional uncertainty of 3%–8% in $\alpha_1\alpha_2 G$.

A similar analysis applied to $\alpha_1\alpha_2$, as determined by (8), indicates that the fractional uncertainty in $\alpha_1\alpha_2$ is approximately 0.5%, which is small compared to the rest of (14). Referring back to (14), we see that $u(G)/G$ is approximately equal to the root sum of squares of $u(\alpha_1\alpha_2 G)/\alpha_1\alpha_2 G$ and $u_{\rm ML}(G)/G$. This yields a fractional uncertainty from 3% to about 8%, in approximate agreement with Table I.

In computing T_e in (13), we use $\alpha_1\alpha_2 G^2 = (\alpha_1\alpha_2 G)^2/\alpha_1\alpha_2$, thus writing T_e in terms of quantities ($\alpha_1\alpha_2 G$ and $\alpha_1\alpha_2$) that are independently measured. This avoids the strong correlations that would be present between the errors in $\alpha_1\alpha_2$ and G. The uncertainty in T_e is then obtained from

$$\begin{aligned}\frac{u^2(T_e+T_{He}+T_{\rm vac})}{(T_e+T_{He}+T_{\rm vac})^2} &= \frac{1}{4}\frac{u^2\left(T_O(4d)-\Delta T_2\right)}{\left(T_O(4d)-\Delta T_2\right)^2} + \frac{1}{4}\frac{u^2\left(T_I(4e)-\Delta T_1\right)}{\left(T_I(4e)-\Delta T_1\right)^2} \\ &\quad + \frac{1}{4}\frac{u^2(\alpha_1\alpha_2)}{(\alpha_1\alpha_2)^2} + \frac{u^2(\alpha_1\alpha_2 G)}{(\alpha_1\alpha_2 G)^2} \\ &\quad + \frac{(T_e+T_{He}+T_{\rm vac})^2 u_{\rm ML}^2(T_e)}{T_e^2}. \end{aligned} \tag{16}$$

Since the uncertainty in $T_{He} + T_{\rm vac}$ is negligible, $u(T_e) \approx u(T_e + T_{He} + T_{\rm vac})$, and we can get $u(T_e)$ directly from (16). From the discussion of $u(G)$ above, we know that $u(\alpha_1\alpha_2 G)/\alpha_1\alpha_2 G$ is about 3%–8%, and $u(\alpha_1\alpha_2)/\alpha_1\alpha_2$ is considerably smaller than that. The first two terms on the right-hand side of (16) are both roughly $(0.008)^2$, so that neglecting the matching uncertainties, $u(T_e) \approx 0.04(T_e + T_{He} + T_{\rm vac}) \approx 0.3$ K. To this we must add the effect of possible errors due to imperfections of the matched loads $u_{\rm ML}(T_e)$. The uncertainty in T_e due to imperfect matching conditions is difficult to estimate because we do not know the full noise parameters of the amplifier under test. We can, however, make reasonable estimates of their magnitudes based on the measured value of T_e. Those estimates led us to use

$$\frac{u_{\rm ML}(T_e)}{T_e} \approx \sqrt{4|\Gamma_{\rm ML}|^2 + 2|\Gamma_{\rm ML} S_{11}|^2} \tag{17}$$

which ranges from less than 1% to 8.5% over the 1–12-GHz range. This uncertainty was added in quadrature with the value of $u(T_e)$ obtained from (16), resulting in the uncertainties of Table I. For frequencies at which $|\Gamma_{\rm ML}|$ is sufficiently small, the uncertainty is 0.3 K; at other frequencies, (17) is appreciable or even dominant.

D. Discussion

Repeatability of connectors and cables under cryogenic conditions may have caused some problems. In particular, the 2% differences seen between measurements of the amplifier output at the same frequency with two different receiving modules may have been due to the connectors or cables, since measurements in the different bands were made several weeks apart and involved breaking of connections and heating and recooling. (Usually the repeatability of such measurements is about 0.5% or better.) In future measurements, we will try to use PC-3.5 connectors in place of the SMA connectors used in these measurements. We will also attempt to use better cables and matched loads in order to achieve the best uncertainties over a wider range of frequencies.

Since the amplifier must be measured in three different configurations, and therefore in at least three different cooling/warming cycles, it is important that the amplifier's properties remain the same from cycle to cycle. We did not systematically study this question, but there is considerable evidence that the amplifier properties repeat well. The two sets of VNA measurements in Fig. 5 were made a month apart and agree very well with each other. Also, noise measurements at the radiometer's overlap frequencies (2, 4, and 8 GHz) were often made in different cooling/warming cycles on the different receiver modules. The 2% differences noted above could have been due at least in part to changes in the amplifier. However, differences between the two measurements are included in the overall uncertainties. Thus, in Figs. 5, 7, and 9, the fact that the uncertainties at 2, 4, and 8 GHz are not noticeably larger than at other frequencies is an indication that any variation in the amplifier's properties from one cycle to another is small compared to other uncertainties.

A key point is the temperature of the matched load on the amplifier input in configurations 4(d) and (e). The matched load is immersed in liquid helium and connected directly to the amplifier input, and the amplifier block is mounted through indium sheets on the cold plate. The temperature of the cold plate is monitored by the GRT, with an uncertainty of about 0.05 K, and is checked by the silicon thermometer. Consequently, the temperature of the matched load is known very well. Furthermore, in configurations 4(d) and (e), there is no cable connecting the matched load to an external port, and thus there is no danger of the center conductor heating the matched load. This is an attractive feature of the present method. For cables connected to an external port [see configurations 3 and 4(a)–(c)], the temperature of the center conductor may be higher than 4.1 K because the center conductor is not in contact with the liquid helium, and the thermal contact between the inner and outer conductor may not be very good, but configurations 4(b) and (c) are only used to determine ΔT_1 and ΔT_2, where relatively large errors in the temperature of the matched load can be tolerated. And configuration 4(a) is used to correct for the line losses in configuration 3, so we only need the line temperatures to be the same in the two configurations.

An obvious question that arises is why we were able to achieve such small uncertainties in measuring the amplifier's noise temperature. The key point is the use of a liquid-helium temperature matched load directly on the input of the amplifier, and the measurement of the output noise through both (input and output) cryostat lines [see Fig. 4(d) and (e)]. This provides a very accurately known input noise temperature, and the uncertainties in the gain and line characterization enter as *fractional* uncertainties, contributing to the fractional uncertainty in T_e. The gain and line loss can be measured to within a few percent with accurate noise measurements. Our fractional uncertainty in T_e is actually rather large, but because T_e is so small, the absolute uncertainty is small. It also helps that the method is not very sensitive to the noise added by the lines, ΔT_1 and ΔT_2, which are difficult to measure accurately.

Some aspects of the present method could be used to improve the accuracy of other methods, such as those used in [7]. Careful characterization of, and correction for, the noise properties of the cables would reduce the uncertainties, but at the expense of added measurements and cooling/warming cycles. We think that there still would be an advantage to our method of first measuring the gain with external noise sources and then determining the noise temperature with just one internal matched load, but we cannot say definitely without a detailed analysis.

There are possibilities for making the present method somewhat faster. The fact that the present method is relatively insensitive to the noise added by the lines (ΔT_1 and ΔT_2) suggests a possible shortcut method similar to that proposed, but requiring fewer internal configurations and fewer noise measurements. The quantities $\alpha_1\alpha_2 G$ and $\alpha_1\alpha_2$ could be determined from VNA measurements alone (provided the VNA measurement of S_{21} has sufficient accuracy for large values of $\alpha_1\alpha_2 G$). Furthermore, the configurations of Fig. 4(b) and (c) could be omitted if it could be verified that ΔT_1 and ΔT_2 were negligible compared to GT_e. This might be done by noting that ΔT_1 and ΔT_2 must be bounded above by $(1-\alpha_1)T_{\rm amb}$ and $(1-\alpha_2)T_{\rm amb}$.

Another possible efficiency in the present method could be achieved by building a dedicated test setup and characterizing the lines once (with periodic checks). The line characterization measurements would then not need to be done each time a new device was measured. We intend to build such a test setup in the near future.

IV. Summary

We have proposed and applied a method for measuring the effective input noise temperature of a cryogenic (liquid-helium temperature) amplifier under matched conditions. The method uses a basic hot/cold measurement to determine the gain of the amplifier between the cryostat's input and output ports. Replacing the amplifier with a through section and performing a similar hot/cold measurement to determine the loss in the lines between the internal reference planes and the cryostat's input and output ports enabled us to determine the amplifier's gain between its input and output reference planes within the cryostat. Once the gain was known, the amplifier's noise temperature was determined by measurements using a matched load connected directly to the amplifier input within the cryostat, and therefore at liquid-helium temperature. Additional measurements determined the noise added by the lines connecting the amplifier to the cryostat ports. This method (and a careful uncertainty analysis) enabled us to measure the effective amplifier input noise temperature with an uncertainty of ± 0.3 K at frequencies for which the nominal matched loads were well matched, which is about equal to the input noise contribution of the quantum vacuum fluctuations (0.29 K) at the upper end of the frequency range measured (12 GHz).

There are two noteworthy aspects of the results. One is the outstanding noise performance of the amplifier over a full decade of frequency. Its measured noise temperature was below 5.5 K from 1 to 11 GHz, with a minimum of 2.3 K at 7 GHz. The second noteworthy point is that we were able to measure such small amplifier noise temperatures with an estimated standard uncertainty of only 0.3 K. Such accuracy should benefit any application of cryogenic amplifiers, including the terahertz receiver application, which prompted this study. With the recent development of near quantum-limited terahertz detection systems, the need for precise characterization of cryogenic LNAs is higher than ever. The method presented here should enhance the development of focal-plane-array imagers and spectrometers based on heterodyne detectors covering the entire terahertz frequency range.

Appendix

The available power ratio from plane 2 to plane O in Fig. 3 or Fig. 4(a) is given by

$$\alpha_{O2} = \frac{|S_{21}(O2)|^2\left(1-|\Gamma_2|^2\right)}{|1-\Gamma_2 S_{11}(O2)|^2\left(1-|\Gamma_O|^2\right)}. \qquad \text{(A.1)}$$

For configuration Fig. 4(a), with an ambient-temperature matched load on plane I, all reflections are small ($|\Gamma|^2$, $|S_{11}|^2 \approx 0.001$ or less), and thus $\alpha_{O2} \approx |S_{21}(O2)|^2$. We use α_2 to refer to this reflectionless case, $\alpha_2 \equiv \alpha_{O2}(4a)$.

When the amplifier is present, as in Fig. 3, $|\Gamma_2|^2$ and $|\Gamma_O|^2$ are sometimes as large as 0.09, and we must therefore account for them in (A.1) if we are to achieve the accuracy we desire. In such a case, $S_{11}(O2)$ still refers to the section of transmission line, not the amplifier, and $\Gamma_2 S_{11}(O2)$ is still small enough to neglect. We measure Γ_O, and we can write Γ_2 (which we can not measure) in terms of Γ_O as follows:

$$\begin{aligned}\Gamma_O &= S_{22}(O2) + \frac{S_{12}(O2)S_{21}(O2)\Gamma_2}{1 - S_{11}(O2)\Gamma_2} \\ &\approx S_{12}(O2)S_{21}(O2)\Gamma_2 \\ |\Gamma_2|^2 &\approx \frac{|\Gamma_O|^2}{\alpha_2^2}. \end{aligned} \tag{A.2}$$

Therefore, α_{O2} of Fig. 3, denoted $\alpha_{O2}(3)$, is related to $\alpha_{O2}(4a) \equiv \alpha_2$ by

$$\alpha_{O2}(3) \approx \alpha_2 \frac{\left(1 - \dfrac{|\Gamma_O(3)|^2}{\alpha_2^2}\right)}{\left(1 - |\Gamma_O(3)|^2\right)} \approx \alpha_2 \frac{\left(1 - \dfrac{|\Gamma_O(3)|^2}{\alpha_1\alpha_2}\right)}{\left(1 - |\Gamma_O(3)|^2\right)}. \tag{A.3}$$

In evaluating (A.3), we were able to use $\alpha_2^2 \approx \alpha_1\alpha_2$ because the additional error introduced is a small correction to a small correction and therefore negligible. The same value of $\alpha_{O2}(3)$ is used for both noise sources. This is justified because our measurements verified that $|\Gamma_2(3)|^2$ is the same for both.

In a similar manner, we can show that the other α's involving the amplifier are given by

$$\begin{aligned}\alpha_{O2}(4d) &\approx \alpha_2 \frac{\left(1 - \dfrac{|\Gamma_O(4d)|^2}{\alpha_1\alpha_2}\right)}{\left(1 - |\Gamma_O(4d)|^2\right)} \\ \alpha_{I1}(4e) &\approx \alpha_1 \frac{\left(1 - \dfrac{|\Gamma_I(4e)|^2}{\alpha_1\alpha_2}\right)}{\left(1 - |\Gamma_I(4e)|^2\right)} \end{aligned} \tag{A.4}$$

where we define α_1 as we did α_2, $\alpha_1 \equiv \alpha_{I1}(4a)$.

ACKNOWLEDGMENT

The authors thank S. Weinreb and N. Wadefalk, both of the Jet Propulsion Laboratory, California Institute of Technology, Pasadena, for providing the MMIC chip and S. Yngvesson and F. Rodriguez-Morales, both of the University of Massachusetts, Amherst, for their collaboration.

REFERENCES

[1] J. C. Weber and M. W. Pospieszalski, "Microwave instrumentation for radio astronomy," *IEEE Trans. Microw. Theory Tech.*, vol. 50, no. 3, pp. 986–995, Mar. 2002.

[2] M. W. Pospiszalski, "Extremely low-noise amplification with cryogenic FET's and HFET's: 1970–2004," Ferdinand-Braun-Inst. Höchstfrequenztech., Berlin, Germany, Res. Rep., vol. 3, 2005.

[3] ——, "Extremely low-noise amplification with cryogenic FET's and HFET's: 1970–2004," Nat. Radio Astronomy Observatory, Charlottesville, VA, Electron. Div. Int. Rep. 314, May 16, 2005. [Online]. Available: http://www.gb.nrao.edu/electronics/edir/edir314.pdf.

[4] E. Gerecht, C. Musante, Y. Zhuang, K. S. Yngvesson, T. Goyette, J. Dickinson, J. Waldman, P. Yagoubov, G. Gol'tsman, B. Voronov, and E. Gershenzon, "NbN hot electron bolometric mixers, a new technology for low-noise THz receivers," *IEEE Trans. Microw. Theory Tech.*, vol. 47, no. 12, pp. 2519–2527, Dec. 1999.

[5] I. Lopez-Fernandez, J. D. Gallego-Puyol, C. Diez, and J. Martin-Pintado, "Wide band, ultra low noise cryogenic InP IF amplifiers for the Herschel mission radiometers," *Proc. SPIE—Int. Soc. Opt. Eng.*, vol. 4855, pp. 489–500, Aug. 2002.

[6] I. Angelov, N. Wadefalk, J. Stenarson, E. Kollberg, P. Starski, and H. Zirath, "On the performance of low noise, low DC power consumption cryogenic amplifiers," *IEEE Trans. Microw. Theory Tech.*, vol. 50, pp. 1480–1486, Jun. 2002.

[7] N. Wadefalk *et al.*, "Cryogenic wide-band ultra-low-noise IF amplifiers operating at ultra-low DC power," *IEEE Trans. Microw. Theory Tech.*, vol. 51, no. 6, pp. 1705–1711, Jun. 2003.

[8] F. Rodriguez-Morales, K. S. Yngvesson, E. Gerecht, N. Wadefalk, J. Nicholson, D. Gu, X. Zhao, T. Goyette, and J. Waldman, "A terahertz focal plane array using HEB superconducting mixers and MMIC IF amplifiers," *IEEE Microw. Wireless Compon. Lett.*, vol. 15, no. 4, pp. 199–201, Apr. 2005.

[9] H. B. Callen and T. A. Welton, "Irreversibility and generalized noise," *Phys. Rev.*, vol. 83, no. 1, pp. 34–40, Jul. 1951.

[10] C. M. Caves, "Quantum limits on noise in linear amplifiers," *Phys. Rev. D*, vol. 26, no. 8, pp. 1817–1839, Oct. 1982.

[11] J. R. Tucker and M. J. Feldman, "Quantum detection at millimeter wavelengths," *Rev. Mod. Phys.*, vol. 57, no. 4, pp. 1055–1113, Oct. 1985.

[12] A. R. Kerr, "Suggestions for revised definitions of noise quantities, including quantum effects," *IEEE Trans. Microw. Theory Tech.*, vol. 47, no. 3, pp. 325–329, Mar. 1999.

[13] C. Grosvenor, J. Randa, and R. L. Billinger, "Design and resting of NFRad—A new noise measurement system," NIST, Boulder, CO, Tech. Note 1518, Mar. 2000. [Online]. Available: http://www.boulder.nist.gov/div818/81801/Noise/publications/noise_pubs.html.

[14] *ISO Guide to the Expression of Uncertainty in Measurement*. Geneva, Switzerland: Int. Org. Standard., 1993.

[15] J. D. Gallego and M. W. Pospieszalski, "Accuracy of noise temperature measurement of cryogenic amplifiers," Nat. Radio Astron. Observatory, Charlottesville, VA, Electron. Div. Int. Rep. 285, Apr. 1991. [Online]. Available: http://www.gb.nrao.edu/electronics/edir/edir285.pdf.

James Randa (M'89–SM'91) received the Ph.D. degree in physics from the University of Illinois at Urbana-Champaign, in 1974.

He then held post-doctoral and/or faculty positions with Texas A&M University, College Station, the University of Manchester, Manchester, U.K., and the University of Colorado at Boulder. During this time, he performed research on the phenomenology of elementary particles and on theories of fundamental interactions. Since 1983, he has been with what is now the Electromagnetics Division, National Institute of Standards and Technology (NIST), Boulder, CO. From 1983 to 1994, he was with the Fields and Interference Metrology Group, involved with various topics in electromagnetic interference (EMI) metrology. Since 1994, he has been with the RF Electronics Group, NIST, where he heads the Thermal Noise Metrology Project.

Eyal Gerecht (S'88–M'98) received the B.S.E.E. degree in electrical engineering (*magna cum laude*) (with a minor in solid-state physics) from the University of Houston, Houston, TX, in 1990, and the M.S.E.C.E and Ph.D. degrees in electrical and computer engineering from the University of Massachusetts at Amherst, in 1994 and 1998, respectively.

In 1998, he joined the Department of Physics and Astronomy, University of Massachusetts at Amherst, as a Senior Post-Doctoral Research Associate. Since 2000, he has been a Physicist with the Electromagnetics Division, National Institute of Standards and Technology (NIST), Boulder, CO, where he develops numerous terahertz-related technologies. His interests also include the development of receivers for millimeter and submillimeter applications.

Dr. Gerecht is a member of Tau Beta Pi and Eta Kappa Nu.

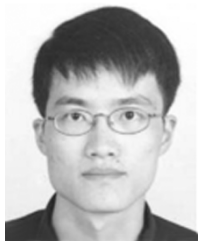

Dazhen Gu (S'01) received the B.S. degree in physics from Nanjing University, Nanjing, China, in 1999, the M.S. degree in electrical engineering from the University of Massachusetts at Amherst, in 2004, and is currently working toward the Ph.D. degree in electrical engineering at the University of Massachusetts at Amherst.

From 1999 to 2001, he was a Research Assistant with the Superconductor Electronics Laboratory, Nanjing University, where he was involved with the three-terminal device employing high-Tc superconductor, ferroelectric, and ferromagnetic materials. Since 2001, he has been involved with the design and fabrication of an NbN hot electron bolometric mixer for terahertz receivers. Since November 2003, he has been with the Electromagnetics Division, National Institute of Standards and Technology (NIST), Boulder, CO, where he is engaged in the development of terahertz imaging systems and characterization of LNAs. His research interest includes nanofabrication, quantum electronics, and RF circuit design.

Robert L. Billinger received the Associates degree in electronics technology from Wichita Technical Institute, Wichita, KS, in 1979.

From 1979 to 1984, he was with the PureCycle Corporation, where he became Manager of Mechanical and Electronic Production and Test. Since 1985, he has been with the Electromagnetics Division, RF Electronics Group, National Institute of Standards and Technology (NIST), Boulder, CO, where he is an Electronics Technician involved in the area of thermal noise.